COMMUNICATIONS IN NUMERICAL METHODS IN ENGINEERING
Commun. Numer. Meth. Engng 2008; **24**:543–553
Published online 20 November 2006 in Wiley InterScience (www.interscience.wiley.com). DOI: 10.1002/cnm.956

Propagation of longest-edge mesh patterns in local adaptive refinement

J. P. Suárez[1,*,†], A. Plaza[2] and G. F. Carey[3]

[1]*Department of Cartography and Graphic Engineering, University of Las Palmas de Gran Canaria, Spain*
[2]*Department of Mathematics, University of Las Palmas de Gran Canaria, Spain*
[3]*Institute for Computational Engineering and Sciences (ICES), The University of Texas at Austin, U.S.A.*

SUMMARY

We examine the propagation of local adaptive mesh refinement (AMR) under a longest edge conformity scheme. Supporting numerical studies are included and discussed. Of specific interest is the statistical behaviour of the propagation zone in AMR of simplicial meshes. To this end three propagation metrics are used: the total number of original triangles in the propagation paths emanating from any target element, the longest individual edge path, and the extent of secondary refinement due to the conformity. Copyright © 2006 John Wiley & Sons, Ltd.

Received 18 May 2006; Revised 24 September 2006; Accepted 5 October 2006

KEY WORDS: adaptive mesh refinement; longest edge propagation statistics

1. INTRODUCTION

Adaptive mesh refinement (AMR) is an established strategy for efficient reliable and accurate simulation [1–4]. In the present work we consider local refinement of simplex elements accompanied by continued longest edge (LE) subdivision of neighbour simplices to ensure conformity. Such LE partitions of triangles are motivated by the desire to maintain conformity of the mesh and simultaneously avoid degradation in mesh quality [2, 5, 6]. Our focus here is the extent of the subsidiary-induced refinement from the target subdivided elements [7]. This is an issue of practical

*Correspondence to: J. P. Suárez, Department of Cartography and Graphic Engineering, University of Las Palmas de Gran Canaria, Spain.
†E-mail: jsuarez@dcegi.ulpgc.es

Contract/grant sponsor: Sandia National Laboratory; contract/grant number: PI2003/35
Contract/grant sponsor: Spanish Ministerio de Ciencia y Tecnología; contract/grant number: MTM2005-08441-C02-02
Contract/grant sponsor: Gobierno de Canarias
Contract/grant sponsor: ICES
Contract/grant sponsor: CFDLab

concern since it has been noted that refinement of a single cell can propagate LE subdivisions to the boundary. Moreover, pathological meshes can be constructed such that refining one target element in this way induces LE refinement in every other element [8–10].

In a previous study, we determined two asymptotic properties induced by LE propagation under uniform refinement [7]. A key goal of the present study is to examine the statistical behaviour of LE secondary mesh refinement under AMR. This will then allow us to infer the expected impact on the practical use of such LE schemes in AMR. The shape quality of the resulting meshes is also of interest.

In the next section, we first define the propagation measures used for these secondary refinement studies. Results for 2D triangulations subject to repeated random local refinements, and to local refinements in a layer are presented to illustrate the calculation of propagation metrics and their use in two dimensions with local refinement. AMR propagation statistics are then compiled and tabulated for two local subdivision strategies. Next, in Section 3 we present some preliminary LE/AMR results for tetrahedra (tets) in 3D. The main results are summarized with some concluding remarks in Section 4.

2. 2D PROPAGATION

2.1. Propagation metrics

To introduce the LE propagation scheme and metrics, let us consider a target triangle t that is to be refined to a quartet of subtriangles by introducing midedge nodes. Conformity of the resulting mesh with adjacent elements can be preserved by continuing refinement of the neighbours as indicated by the arrows in Figure 1(a). Here, rather than simply join new edge nodes to opposite vertices which may yield small angles, we enforce a consistent LE strategy that may consequently propagate some distance into the mesh. The propagation concludes with a terminating triangle pair that share their respective LEs or the boundary. The resulting propagated mesh for this simple case with well-shaped triangles is shown in Figure 1(b). Note that the propagation pattern here is the same if a self-similar subdivision is applied to the initial target triangles.

Two metrics (denoted $M1$ and $M2$) are introduced to quantify secondary propagation in the 2D studies and a third related metric X is constructed and used for the 3D studies in Section 3.

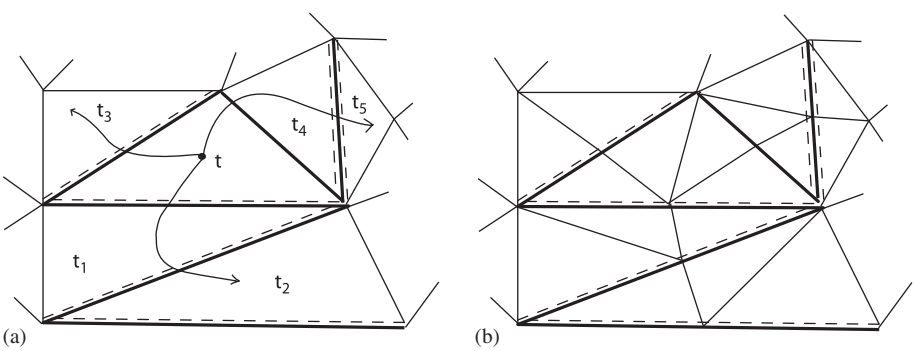

Figure 1. (a) Example with propagation paths indicated by arrows (dashed edges represent longest edges); and (b) 4T-LE refinement of triangulation in (a).

DOI: 10.1002/cnm

Let $M1(t)$ be the total number of original triangles in the propagation paths emanating from t and $M2(t)$ be the longest individual edge path from t. Hence, $M1(t) = 5$ and $M2(t) = 2$ in the preceding example. The excess is $X = 13 - 5 = 7$ in the example since induced secondary refinement introduces 2 pairs and 3 triples of subelements replacing the 5 neighbours impacted by target refinement. Since we are especially interested in the extent of the secondary refinement we focus on $M1(t)$ and the corresponding number of excess new triangles X in this secondary region. As explained later in Section 3, we use only the excess X in the 3D studies.

The shape of the triangles and the irregularity of nodal valence (the number of elements adjacent to a vertex) clearly influence the behaviour of $M1$ and $M2$. For example, the extent of the conformity zone for the favourable case of a uniform mesh of right triangles is shown in Plate 1, where 5 interior target triangles have been selected and the secondary refinement propagates similarly for each without overlaps. Then $M1 = 5$ and $M2 = 2$ for each target triangle so their means are also, respectively, $\mu(M1) = 5$ and $\mu(M2) = 2$.

2.2. *Repeated random local AMR*

As a first step towards understanding the effect of local repeated refinement on the statistical behaviour of the propagation zone, we conduct numerical experiments with repeated random local refinement. This random local refinement differs from the standard application of local AMR only in the process by which the target cells are selected at each step. (The latter is not random but instead adapts to specific local behaviour of the solution.) The initial meshes considered are a uniform mesh of right triangles, an unstructured Delaunay triangulation, and a mesh of slender triangles in a pentagonal geometry. The algorithm for the numerical experiment in each case involves sampling a target triangle from the current (evolving) mesh and computing propagation metrics and statistics as follows:

1. Select a triangle (at random) in the current mesh.
2. Refine this triangle.
3. Determine the propagating region values $M1$, $M2$ and X for each triangle in the mesh.
4. Update the values for evolving propagation measure statistics (compute averages for $M1$, $M2$ and X).
5. Stop if sampling complete or return to step 1.

In uniform LE refinement we have a balanced refinement tree and have previously shown that the average propagation zone for each triangle is progressively reduced at each uniform refinement stage, and asymptotically, approaches five neighbour triangles [7]. In this local random refinement, as in AMR, we generate an unbalanced refinement tree with, typically, some elements at root level zero, some at the next level one, and so on to the 'leaves' at the finest refinement level. This naturally destroys the 'regularity' of the mesh so one might expect to encounter relatively large values for the propagation zone. The following test cases are designed to investigate this point.

The initial test meshes and final refined meshes after 329 'samplings' are shown in Figure 2. The final mesh means, standard deviation, Min(m) and Max(M) values for $M1$, $M2$ and X are given in Table I. As seen from the mean values of X for each mesh given in the table, approximately 15 additional triangles are generated per refinement. The largest value of X is 46 triangles for the 'Pentagonal' mesh, because the initial mesh contains many slender triangles. However, the mean values do decline very rapidly when refinement is activated and this pathological structure is disrupted by LEPP (e.g. $\mu(M1) = 26.5$ drops to 6.9 at step 2, and it stabilizes at 7.06 when the

DOI: 10.1002/cnm

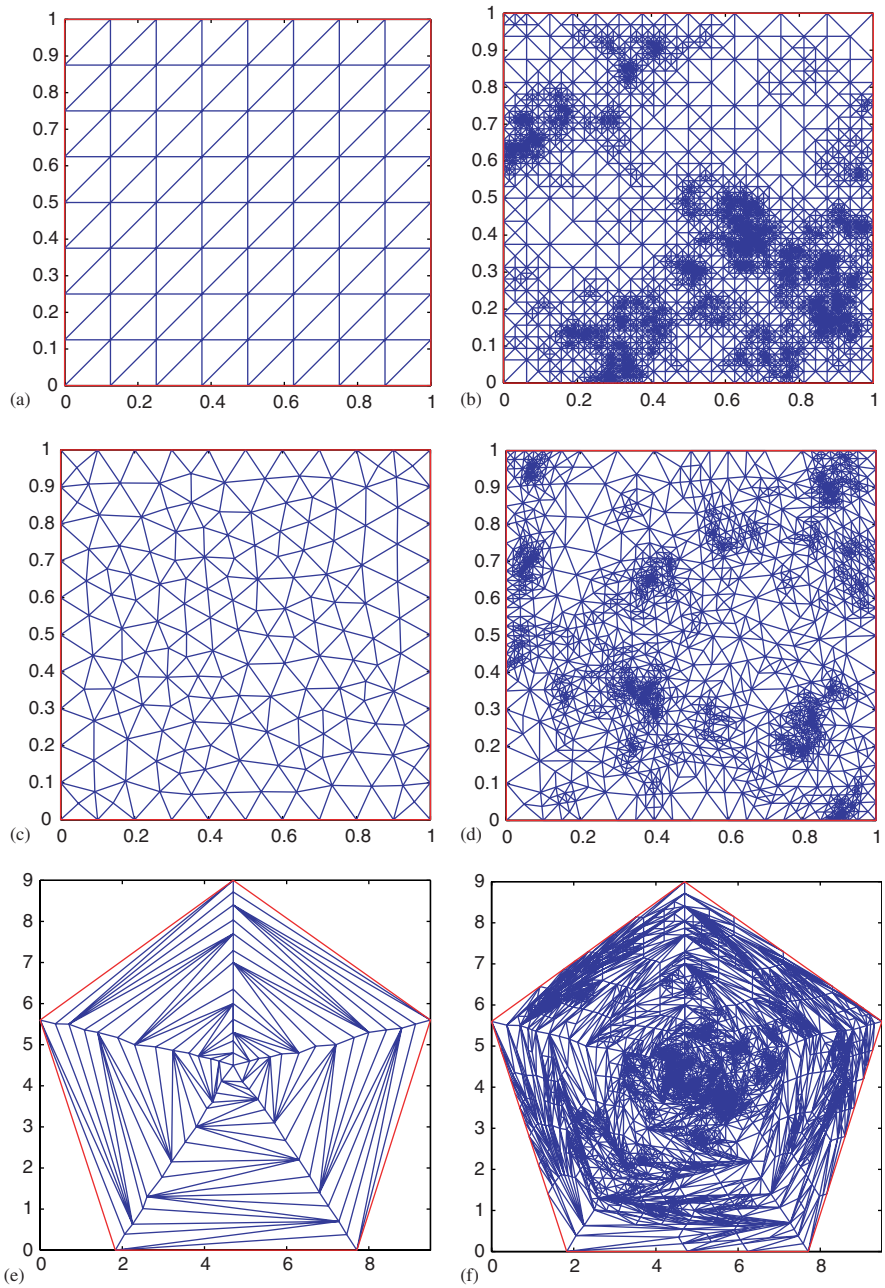

Figure 2. Initial and refined meshes with repeated random local AMR. Right-triangle-type mesh: (a) initial mesh with 128 triangles; and (b) final mesh after 329 refinement steps. Delaunay-type mesh. (c) initial mesh with 328 triangles; and (d) final mesh after 329 refinement steps. Pentagonal-type mesh. (e) initial mesh with 125 triangles; and (f) final mesh after 329 refinement steps.

DOI: 10.1002/cnm

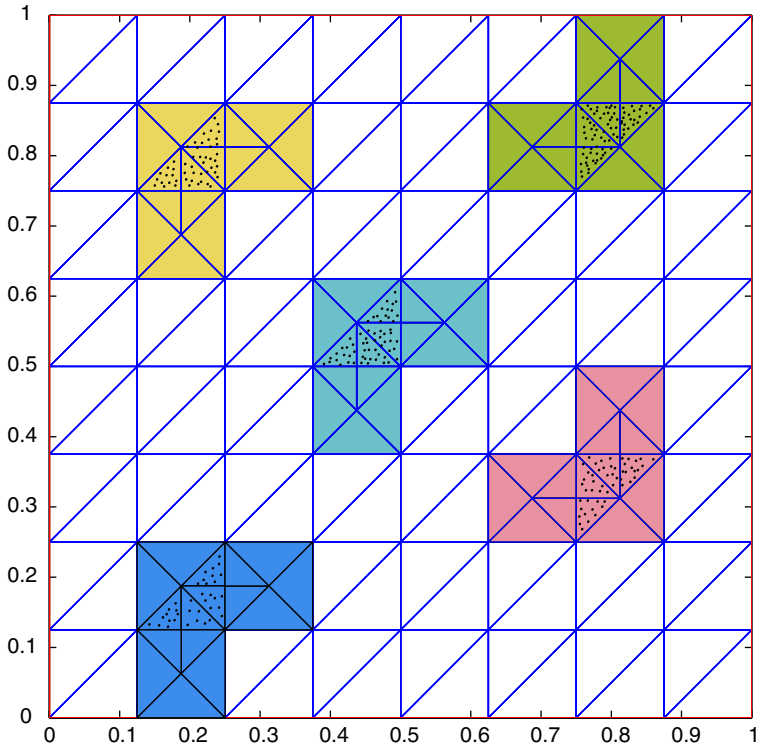

Plate 1. Local refinement and propagation zone in colours.

DOI: 10.002/cnm

Table I. Element excess X, $M1$ and $M2$ statistics: average (μ), standard deviation (S), min (m) and max (M) from 329 sample steps.

	X				$M1$				$M2$			
	μ	S	m	M	μ	S	m	M	μ	S	m	M
Right-triangle mesh	14.64	5.38	5	36	7.27	2.64	2	19	3.61	1.48	1	11
Delaunay mesh	15.13	5.19	5	36	7.17	2.68	2	21	3.61	1.48	1	12
'Pentagonal' mesh	14.60	5.55	6	46	7.06	2.61	2	74	3.64	1.67	2	26

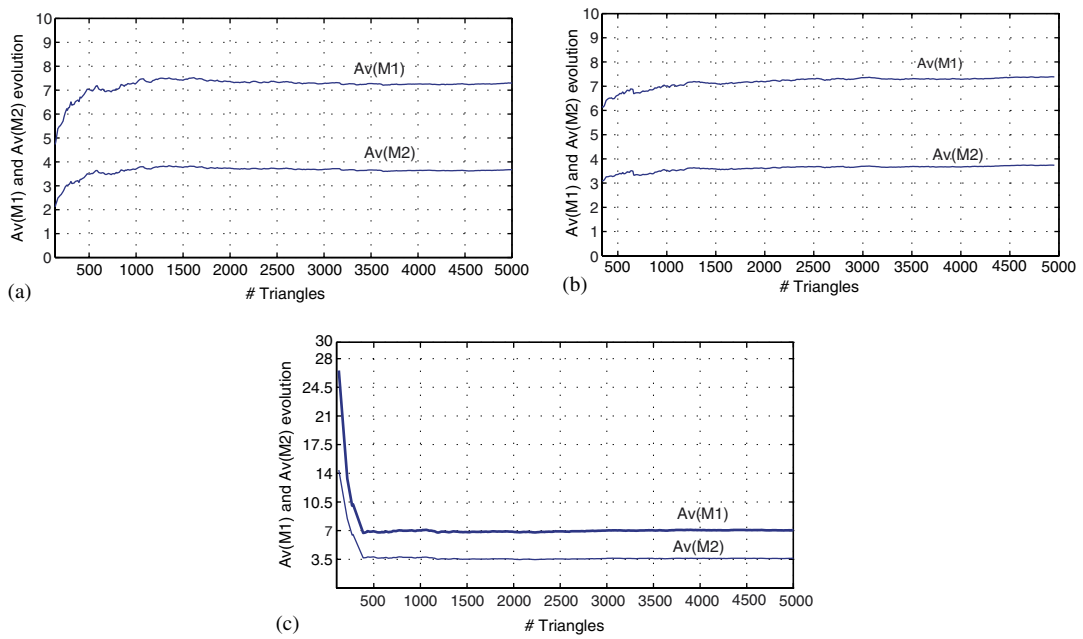

Figure 3. Averages of $M1$ and $M2$ for random sample triangle selection: (a) right triangle mesh with random sample triangle selection. 4T-LE; (b) Delaunay-type mesh with random sample triangle selection. 4T-LE; and (c) pentagonal mesh with random sample triangle selection. 4T-LE.

refinement continues). The evolution of the mesh properties as random local refinement continues is indicated in Figure 3 and we see that the means $\mu(M1)$ and $\mu(M2)$ approach 7 and 3.6, respectively. Several other examples for different meshes (not shown here) were tested and revealed similar results. In view of this, we infer that the behaviour of $\mu(M1)$ and $\mu(M2)$ in the refined meshes asymptotically converges to small values depending on the refinement process itself and not on the quality of the initial mesh.

Remark

A similar numerical experiment was carried out for refinement of the patches of elements adjacent to randomly selected nodes for the previous Delaunay mesh in a square domain. As expected,

DOI: 10.1002/cnm

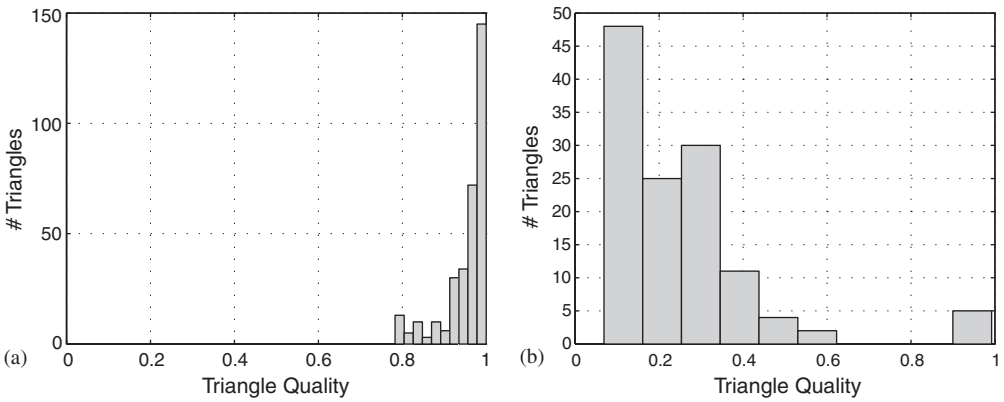

Figure 4. (a) Histogram of initial mesh quality in Delaunay-type mesh (328) triangles; and (b) histogram of initial mesh quality in pentagonal mesh (125 triangles).

the same qualitative behaviour was observed as in the random cell refinement case. In [7] similar results were obtained with the 'pentagonal' mesh in a uniform refinement scenario.

The effect on mesh quality is also of interest. In Figures 4(a) and (b) histograms of a standard cell quality measure are graphed for the initial Delaunay and 'Pentagonal' meshes shown in Figure 2. The mesh quality measure is $q = 4\sqrt{3} \cdot A/(h_1^2 + h_2^2 + h_3^2)$ where A is the area, and h_1, h_2 and h_3 are respective side lengths of each triangle. Here, $q \in [0, 1]$, with $q = 1$ corresponding to the equilateral triangle. In practice, $q > 0.6$ might be taken as an acceptable value for well-shaped triangles [11]. As shown in Figure 4, most of the triangles in the initial Delaunay-type mesh have high shape quality with q near 1. In contrast, almost all the triangles in the 'Pentagonal' mesh are of poor quality. (Remark: triangles in the right isosceles initial mesh of Figure 2 have a constant value in this measure of 0.87.)

We also report in Figure 5 the average mesh quality behaviour for 4T-LE. (The hybrid scheme is not shown since the plots are very close.) In the Delaunay mesh, initial triangles are close to equilateral so average quality initially decreases, from 0.9 to 0.8 approximately, and mesh quality remains around 0.8 as refinement proceeds. Mesh improvement is observed for the 'Pentagonal' mesh through refinement and is consistent with the improvement properties of the 4T-LE subdivision for obtuse triangles [5, 12]. For the right triangle mesh (not shown in the figure), quality remains constant ($q = 0.87$) since local 4T subdivision only produces right-shaped subtriangles. The standard deviation of the mesh quality asymptotically tends to 0.106, and 0.267, respectively, for the Delaunay mesh and the 'Pentagonal' mesh, while for the right mesh the standard deviation is zero, since all the generated triangles are also right isosceles triangles and hence have the same quality measure.

2.3. Layer AMR propagation statistics

The previous results show the behaviour when the selection of target elements is random. However, in AMR, even though the local refinement is not known in advance, it does inherently have a structure that is determined by the selection of target elements using the underlying solution to an approximation problem. In fact, for problems where the solution has layers or singularities,

DOI: 10.1002/cnm

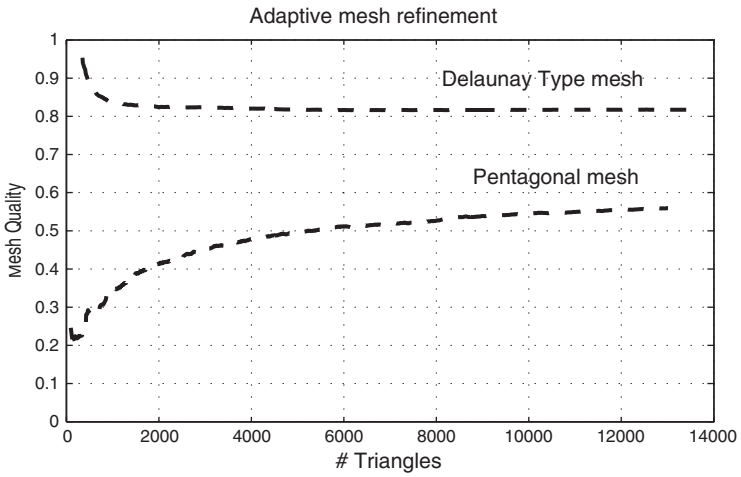

Figure 5. Average mesh quality comparison for Delaunay-type and pentagonal mesh. 4T-LE.

Table II. Local AMR experiment of Plate 2. $M1$ and $M2$ statistics: average (μ); standard deviation (S); min (m) and max (M).

	$M1$				$M2$			
# Refinement step	μ	S	m	M	μ	S	m	M
1	5.74	1.54	2	12	2.69	0.85	2	6
2	5.77	1.58	2	11	2.70	0.86	1	5
3	5.90	1.19	2	13	2.86	0.90	2	9
4	5.83	1.32	2	11	2.78	0.88	2	6
5	5.82	1.40	2	11	2.73	0.91	1	6
6	5.78	1.39	2	11	2.73	0.91	1	6

we expect repeated local refinement to resolve the layers by preferentially refining in these layer subregions. This suggests that the behaviour may exhibit more features similar to local uniform refinement than in the previous random targeting case.

To examine this further we conducted a similar numerical experiment to that above, but using local refinement now targeted to an interior contour. The lines defining the target contours inside a Delaunay-type mesh are shown in Plate 2(a) and align with a subset of edges in the mesh. The elements refined in any step are now those sharing an edge with the interior target contour. Plate 2(b) shows the resulting mesh after four repeated steps of local refinement. Plate 2(c) distinguishes, by colours, the different layers of propagation zones existing at this mesh stage in the refinement process.

Statistical values for $\mu(M1)$ and $\mu(M2)$ are shown in Table II. These values are near 5.8 for $\mu(M1)$ and near 2.7 for $\mu(M2)$ which, as expected, are lower than those obtained in the experiments with the random target selection. Table III presents the propagation area evolution, the number of target triangles to be refined and the triangle excess X resulting from LE propagation.

DOI: 10.1002/cnm

Table III. Propagation in the line singularity example of Plate 2.

Refinement step	Propagation area	Target Triangle (TT)	Excess X	Ratio X/TT
1	0.7739	204	904	4.41
2	0.5443	511	2248	4.39
3	0.2452	1036	4515	4.35
4	0.1213	2080	9098	4.37
5	0.0301	8344	36 660	4.39
6	0.0101	17 184	77 778	4.52

With respect to the excess per triangle in the propagation zone, targeted AMR produces, as expected, lower values to those in the random target case. See last column in Table III.

3. 3D AMR EXPERIMENTS

In the 2D case discussed in Section 2, there is only one neighbouring triangle adjacent to a LE so the propagation path is uniquely determined and measures $M1$, $M2$ easily computed. In 3D a number of neighbouring elements are adjacent to a LE. Hence, multiple refinement paths are possible with more complex and expensive calculations for metrics $M1$ and $M2$ as a consequence. Hence, the number X of excess induced tets is used here as a measure of secondary conforming propagation.

3.1. Sphere domain with interior subdomain

The first 3D test geometry is a sphere Ω_0 containing a concentric smaller sphere Ω_1. An initial conforming tetrahedral mesh is generated for the interior sphere and exterior spherical annulus. For clarity of interpretation, Figure 6(a) shows only the initial wire mesh triangulation for the external boundary of Ω_0 and the interface with Ω_1. In order to visualize the local refinement in the mesh, the graphs in Figure 6(b) and (c) show only the mesh elements whose vertices satisfy the logical expression $(x + y>0)$: for the initial tetrahedral mesh; and, a similar plot after AMR using LE subdivision of the interior sphere. The initial mesh is unstructured with 1747 tets in the spherical annular region exterior to the inner sphere and 180 tets within the small sphere. The target elements in this example are those in the inner sphere Ω_1 and the LE propagation zone extends out into the spherical annular region.

The first experiment can be described as follows: a tet from Ω_1 is selected and then split following a LE approach. The element excess (X) is then computed. After each tet LE refinement is made, we undo the refinement and then a new element within Ω_1 is chosen and split. We proceed in the same manner for every element in Ω_1 until all elements are completed and so an average value for the element excess X is obtained. Since we are interested in how propagation is influenced by repeated refinement, we then apply uniform LE bisection to elements in $\Omega_0 \cup \Omega_1$. This uniform refinement causes elements to be split in two or more tets, as midpoints are placed on the LE of each tet for subdivision. The element excess X is again determined. Table IV shows the results for four steps as described before, where element excess X in average is presented as well as the number of tets resulting in both Ω_0 and the entire mesh. The salient feature from these results is the reduction in average of element excess X. This indicates that the propagation zone is

DOI: 10.1002/cnm

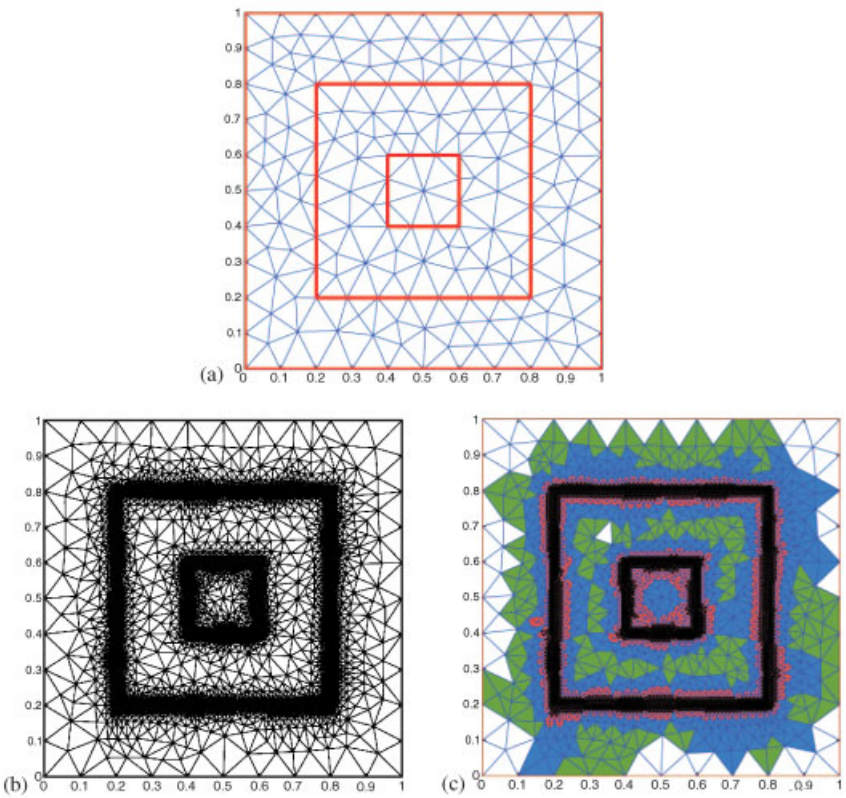

Plate 2. Adaptive mesh refinement in the line singularity problem: (a) initial Delaunay-type mesh with interior constrained lines; (b) locally refined mesh; and (c) colours are used to depict the triangles with different propagating zones.

DOI: 10.002/cnm

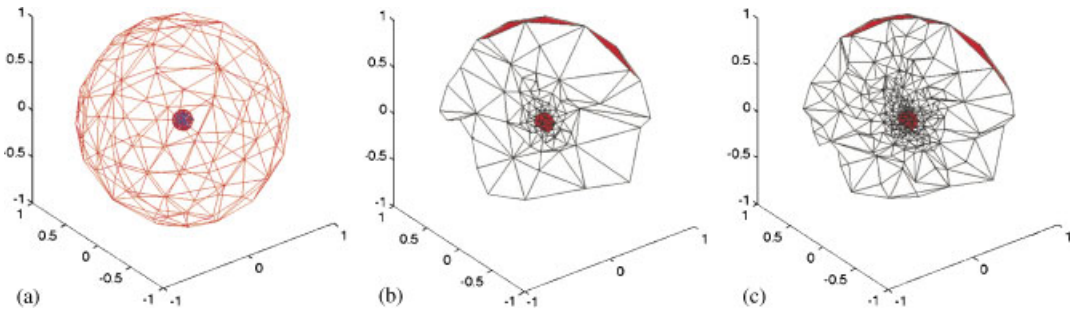

Figure 6. (a) Wire mesh for the boundary of Ω_0 and Ω_1; (b) a plot of initial mesh whose vertices satisfy $x + y > 0$; and (c) a similar plot after AMR using LE subdivision.

Table IV. Sphere domain with interior subdomain.

Step	1	2	3	4
$\mu(X)$	97.70	30.34	21.13	19.90
#Tetrahedra in Ω_1	180	758	2799	9325
#Tetrahedra in $\Omega_0 \cup \Omega_1$	1927	8730	31 209	105 622

Note: Element excess X evolution.

reduced as refinement proceeds, as in the 2D case, but of course with a longer value approaching 20 here in 3D.

We next conduct a similar experiment to that above, but now keep the refinement pattern rather than 'undo' it at each step. Hence, the successive refinements are accumulated as in the 2D studies. After two different tests involving 300 and 500 successive refinement steps we get meshes with 15 982 and 25 023 tets, respectively. On average, the element excess X approaches 35 and 34, respectively.

It is worth noting that for these test cases, the element excess X is still reduced as refinement evolves. Several other similar experiments with Delaunay-type 3D tetrahedral meshes yielded similar results.

We also include here mesh quality measures of meshes generated with the successive tet refinement approach. The mesh quality measure is given by

$$Q = \frac{72\sqrt{3} \cdot V}{(\sum_{i=1}^{6} h_i^2)^{3/2}}$$

where V is the volume of the tet, h_i are the respective sides lengths and $Q \in [0, 1]$ analogous to the 2D quality measure earlier. For the intermediate refined meshes, we graph in Figure 7 the number of tets with quality greater than 0.6 and less than 0.3 as refinement proceeds. It is observed that the number of tets with mesh quality greater than 0.6 (a cut-off quality for a well-shaped tet) linearly increases. Meanwhile, tets with quality less than 0.3 (a poorly shaped tet) remain constant at around 123 tets. This indicates that in addition to the propagation improvement, mesh quality is also proportionally better.

DOI: 10.1002/cnm

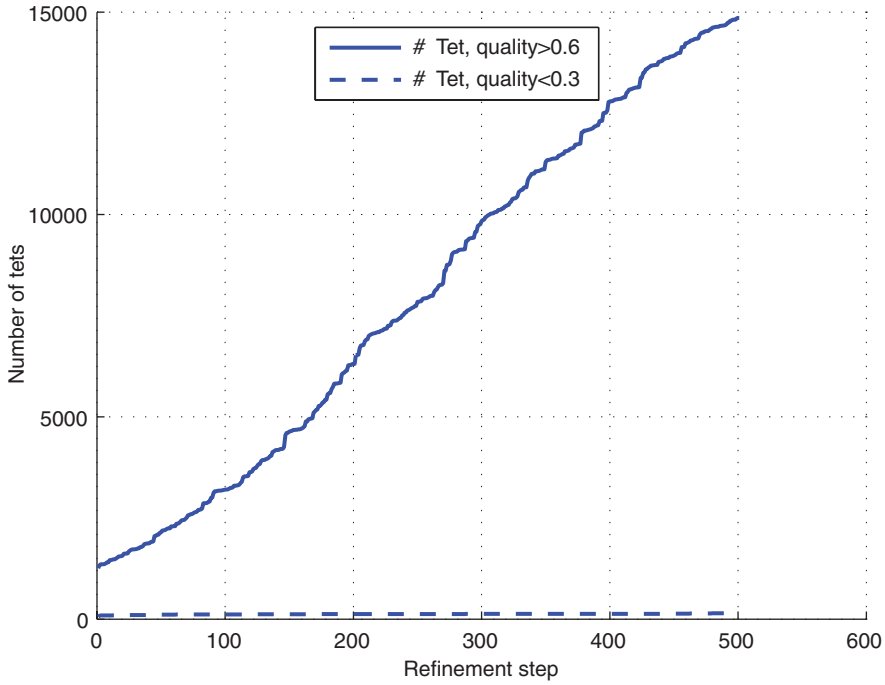

Figure 7. Mesh quality evolution in iterative tet refinement.

4. CONCLUSIONS AND REMARKS

The propagation path behaviour in local LE refinement is relevant to the mesh structure and efficiency of simulations. LE refinement of a single triangle can generate large values for the element excess, $M1$ and $M2$ and the random target local refinement studies show that propagation behaviour as refinement proceeds, appears to be relatively insensitive to the type of initial mesh with mean values approaching those of uniform refinement. In AMR, one typically refines a small percentage of the elements at each refinement step but repeated AMR stages often are focused in specific subregions such as layers or near singularities where the solution is changing significantly. The numerical examples presented in this work demonstrate that the propagation statistics (in terms of $M1$, $M2$ and X) are relatively insensitive to the initial mesh and that average cell quality generally improves or remains well-behaved. It is clear that the AMR situation for $\mu(M1)$ and $\mu(M2)$ cannot be analysed as rigorously as in the uniform case [7], since the refinement is not fully recursive. As might be anticipated, the behaviour of $\mu(M1)$ and $\mu(M2)$ in the highly refined subregions exhibits some of the character of asymptotic values seen in the earlier treatment of uniform refinements, whereas the behaviour on the coarser level mesh subregions will be similar to the pre-asymptotic behaviour. However, the work presented here suggests that, in terms of average behaviour, the adjacent propagation inherent to LE refinement does not constitute a significant obstacle, especially in 2D. The situation with tets exhibits the same trends, but as expected the element excess is much longer and the trends are slower. This suggests that one might control an

DOI: 10.1002/cnm

LE AMR scheme differently in 3D than in 2D. More specifically, because of the more extensive refinement zone a stricter tolerance that would select fewer target cells per AMR step might be appropriate. In fact, this strategy would appear useful even in 2D if one is to compare with other AMR strategies that exploit constraints on hanging nodes of a non-conforming mesh to avoid subsidiary refinement.

ACKNOWLEDGEMENTS

This research has been partially supported by Sandia National Laboratory, the Curran Chair endowment at the University of Texas at Austin, the Gobierno de Canarias grant PI2003/35, and by the Spanish Ministerio de Ciencia y Tecnología, under research CICYT Project MTM2005-08441-C02-02. The first author wants to thank Gobierno de Canarias, ICES and the CFDLab for their financial support during his stay at the University of Texas at Austin.

REFERENCES

1. Bank RE, Sherman A. An adaptive multilevel method for elliptic boundary value problems. *Computing* 1981; **26**(2):91–105.
2. Carey GF. A mesh refinement scheme for finite element computations. *Journal of Computer Methods in Applied Mechanics and Engineering* 1976; **7**(1):93–105.
3. Carey GF. *Computational Grids*: *Generation*, *Adaptation and Solution Strategies*. Taylor & Francis: London, 1997.
4. Hitschfeld N, Villablanca L, Krause J, Rivara MC. Improving the quality of meshes for the simulation of semiconductor devices using Lepp-based algorithms. *International Journal for Numerical Methods in Engineering* 2003; **58**(2):333–347.
5. Rivara MC, Iribarren G. The 4-triangles longest-side partition of triangles and linear refinement algorithms. *Mathematics of Computation* 1996; **65**(216):1485–1502.
6. Rosenberg IG, Stenger F. A lower bound on the angles of triangles constructed by bisecting the longest side. *Mathematics of Computation* 1975; **29**:390–395.
7. Suárez JP, Plaza A, Carey GF. The propagation problem in longest-edge refinement. *Finite Elements in Analysis and Design* 2005; **42**(2):130–151.
8. Bellenger E, Coorevits P. Adaptive mesh refinement for the control of cost and quality in finite element analysis. *Finite Elements in Analysis and Design* 2005; **41**(15):1413–1440.
9. Jones MT, Plassmann PE. Parallel algorithms for adaptive mesh refinement. *SIAM Journal on Scientific Computing* 1997; **18**:686–708.
10. Rivara MC, Vemere M. Cost analysis of the longest-side (triangle bisection) refinement algorithm for triangulation. *Engineering with Computers* 1996; **12**:224–234.
11. Bank RE. *PLTMG*: *A Software Package for Solving Elliptic Partial Differential Equations. Users' Guide 9.0.* Department of Mathematics, University of California, San Diego, 2004.
12. Plaza A, Suárez JP, Padrón MA, Falcón S, Amieiro D. Mesh quality improvement and other properties in the four-triangles longest-edge partition. *Computer Aided Geometric Design* 2004; **21**(4):327–422.

DOI: 10.1002/cnm